VPSNR: Visual Perceptual Full-Reference Image Quality Assessment for JPEG2000

Jaime Moreno, Carlos Correa, Nallely Hernández, Diana Pérez

Superior School of Mechanical and Electrical Engineering
National Polytechnic Institute of Mexico,
IPN Avenue, Lindavista, Mexico City, 07738, Mexico.
XLIM Laboratory, Signal, Image and Communications Department,
University of Poitiers, 86962 Futuroscope, France.
jmorenoe@ipn.mx

Abstract. Estimation of image quality is decisive in the image compression field. This is important in order to minimize the induced error via rate allocation. Traditional full-reference algorithms of image quality try to model how Human Visual System detects visual differences and extracts both information and structure of the image. In this work we propose a quality assessment, which weights the mainstream PSNR (Peak Signal-to-Noise Ratio) by means of a perceptual model (VPSNR). Perceptual image quality is obtained by estimating the rate of energy loss when an image is observed at monotonically increasing distances. Experimental results show that VPSNR is the best-performing algorithm, compared with another eight metrics such as MSSIM, SSIM or VIF, among others, when an image is distorted by a wavelet compression. It has been tested across TID2008 image database.

1 Introduction

Mean Squared Error (MSE) is still the most used quantitative performance metrics and several image quality measures are based on it, being Peak Signal-toNoise Ratio (PSNR) the best example. Wang and Bovik in [1,2] consider that MSE is a poor device to be used in quality assessment systems. Therefore it is important to know what is the MSE and what is wrong with it, in order to propose new metrics that fulfills the properties of human visual system and keeps the favorable features that the MSE has.

In this way, let $f(i,j)$ and $\hat{f}(i,j)$ represent two images being compared and the size of them is the number of intensity samples or pixels. Being $f(i,j)$ the original reference image, which has to be considered with perfect quality, and $\hat{f}(i,j)$ a distorted version of $f(i,j)$, whose quality is being evaluated. Then, the MSE and the PSNR are, respectively, defined as:

Advances in Computer Science and Engineering
Research in Computing Science 63, 2013 pp. 65–79
Paper Recived 21-09-2013 and Acepted 21-10-2013

$$MSE = \frac{1}{NM} \sum_{i=1}^{N} \sum_{j=1}^{M} \left[f(i,j) - \hat{f}(i,j) \right]^2 \quad (1)$$

and

$$PSNR = 10 \log_{10} \left(\frac{{\mathcal{G}_{max}}^2}{MSE} \right) \quad (2)$$

where G_{max} is the maximum possible intensity value in $f(i,j)$ ($M \times N$ size). Thus for gray-scale images that allocate 8 bits per pixel (bpp) $G_{max} = 2^8 - 1 = 255$. For color images the PSNR is defined as in the Equation 2, whereas the color MSE is the mean among the individual MSE of each component. MSE does not need any positional information in the image, thus pixel arrangement is ordered as a one-dimensional vector.

Both MSE and PSNR are extensively employed in the image processing field, since these metrics have favorable properties, such as:

1. A convenient metrics for the purpose of algorithm optimization. For example in JPEG2000, MSE is used both in Optimal Rate Allocation [3,4] and Region of interest [5,4]. Therefore MSE can find solutions for these kind of problems, when is combined with the instruments of linear algebra, since it is differentiable.
2. By definition MSE is the difference signal between the two images being compared, giving a clear meaning of the overall error signal energy.

However, the MSE has a poor correlation with perceived image quality. An example is shown in Figure 1, where both *Baboon*(a) and *Splash*(b) Images are distorted by means of a JPEG2000 compression with 30dB of PSNR. These noisy images present dramatically different visual qualities. Thereby either MSE or PSNR do not reflect the way that human visual system (HVS) perceives the images, since these measures represent an input image in a pixel domain.

(a) Image *Baboon* (b) Image *Splash*

Fig.1. 256×256 patches of Images *Baboon* and *Splash* distorted by means of JPEG2000 both with PSNR=30dB, cropped for visibility.

2 Perceptual peak signal-to-noise ratio

2.1 Introduction

In the referenced image quality issue, there is an original image $f(i,j)$ and a distorted version $\hat{f}(i,j) = \Lambda[f(i,j)]$ that is compared with $f(i,j)$, being Λ a distortion model. The difference between these two images depends on the characteristics of the distortion model Λ. For example, blurring, contrast change, noise, JPEG blocking or wavelet ringing.

In Figure 1, the images *Babbon* and *Splash* are compressed by means of JPEG2000. These two images have the same PSNR=30 dB when compared to their corresponding original image, that is, they have the same numerical degree of distortion (i.e. the same objective image quality PSNR). But, their subjective quality is clearly different, showing the image *Baboon* a better visual quality. Thus, for this example, PSNR and perceptual image quality has a small correlation. On the image *Baboon*, high spatial frequencies are dominant. A modification of these high spatial frequencies by Λ induces a high distortion, resulting a lower PSNR, even if the modification of these high frequencies are not perceived by the HVS. In contrast, on image *Splash*, mid and low frequencies are dominant. Modification of mid and low spatial frequencies also introduces a high distortion, but they are less perceived by the HVS. Therefore, correlation of PSNR against the opinion of an observer is small. Figure 2 shows the diagonal high spatial frequencies of these two images, where they are more high frequencies in image *Baboon*.

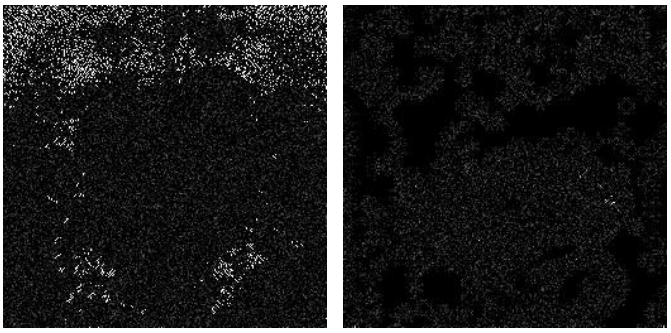

(a) (b)

Fig.2. Diagonal spatial orientation of the first wavelet plane, Images *Baboon*(a) and *Splash*(b) distorted by JPEG2000, PSNR=30dB.

If a set of distortions $\hat{f}_k(i,j) = \Lambda_k[f(i,j)]$ are generated and indexed by k (for example, let Λ be a blurring operator), the image quality of $\hat{f}_k(i,j)$ evolves while varying k, being k, for example, the degree of blurring. Hence, the evolution of $\hat{f}_k(i,j)$ depends on the characteristics of the original $f(i,j)$. Thus, when increasing k,

if $f(i,j)$ contains many high spatial frequencies the PSNR rapidly decreases, but when low and mid frequencies predominated PSNR decreases slowly.

Similarly, the HVS is a system that induces a distortion on the observed image $f(i,j)$, whose model is predicted by The *C*hromatic *I*nduction *Wa*velet *M*odel (CIWaM) [6].

CIWaM takes an input image I and decomposes it into a set of wavelet planes $\omega_{s,o}$ of different spatial scales s (i.e., spatial frequency v) and spatial orientations o. It is described as

$$\mathcal{I} = \sum_{s=1}^{n} \sum_{o=v,h,dgl} \omega_{s,o} + c_n \ , \tag{3}$$

where n is the number of wavelet planes, c_n is the residual plane and o is the spatial orientation either *v*ertical, *h*orizontal or *d*iag*o*na*l*.

The perceptual image I_ρ is recovered by weighting these $\omega_{s,o}$ wavelet coefficients using the *extended Contrast Sensitivity Function* (e-CSF).

Perceptual image I_ρ can be obtained by

$$\mathcal{I}_\rho = \sum_{s=1}^{n} \sum_{o=v,h,dgl} \alpha(\nu, r)\, \omega_{s,o} + c_n \tag{4}$$

where $\alpha(v,r)$ is the e-CSF weighting function that tries to reproduce some perceptual properties of the HVS. The term $\alpha(v,r)\ \omega_{s,o} \equiv \omega_{s,o;\rho,d}$ can be considered the *perceptual wavelet coefficients* of image I when observed at distance d. For details on the CIWaM and the $\alpha(v,r)$ function, see [6].

Hence, CIWaM is considered a HVS particular distortion model $\Lambda \equiv$ CIWaM that generates a perceptual image $\hat{f}_\rho(i,j) \equiv I_\rho$ from an observed image $f(i,j) \equiv I$, i.e $I_\rho = CIWaM[I]$. Therefore, a set of distortions is defined as $\Lambda_k \equiv \text{CIWaM}_d$, being d the observation distance. That is, a set of perceptual images are defined $I_{\rho,d} = \text{CIWaM}_d[I]$ which are considered a set of perceptual distortions of image I.

When images $f(i,j)$ and $\hat{f}(i,j)$ are simultaneously observed at distance $\bar{d}$ and this distance is reduced, the differences between them are better perceived. In contrast, if $f(i,j)$ and $\hat{f}(i,j)$ are observed from a far distance human eyes cannot perceive their differences, in consequence, the perceptual image quality of the distorted image is always high. The distance where the observer cannot distinguish any difference between these two images is $\bar{d} = \infty$. In practice, $\bar{d} = D$ where differences are not perceived and range some centimeters from the position of the observer. Consequently, the less distorted $\hat{f}(i,j)$, that is, the highest the image quality of $\hat{f}(i,j)$), the shorter the distance D.

2.2 Methodology

Let $f(i,j)$ and $\hat{f}(i,j) = \Lambda[f(i,j)]$ be an original image and a distortion version of $f(i,j)$, respectively. VPSNR methodology is based on finding a distance D, where there is no perpetual difference between the wavelet energies of the images $f(i,j)$ and $\hat{f}(i,j)$, when an observer watch them at d centimeters of observation distance. So measuring the PSNR of $\hat{f}(i,j)$ at D will yield a fairer perceptual evaluation of its image quality.

VPSNR algorithm is divided in five steps, which is described as follows:

Step 1: Wavelet transformation

Wavelet transform of images $f(i,j)$ and $\hat{f}(i,j)$ is performed using Eq. 3, obtaining the sets $\{\omega_{s,o}\}$ and $\{\hat{\omega}_{s,o}\}$, respectively. The employed analysis filter is the Daubechies 9-tap/7-tap filter (Table 1).

Table 1. 9/7 Analysis Filter.

Analysis Filter		
i	Low-Pass Filter $h_L(i)$	High-Pass Filter $h_H(i)$
0	0.6029490182363579	1.115087052456994
±1	0.2668641184428723	-0.5912717631142470
±2	-0.07822326652898785	-0.05754352622849957
±3	-0.01686411844287495	0.09127176311424948
±4	0.02674875741080976	

Step 2: Distance D

The total energy measure or the *deviation signature*[7,8] $\bar{\varepsilon}$ is the absolute sum of the wavelet coefficient magnitudes, defined as

$$\bar{\varepsilon} = \sum_{n=1}^{N} \sum_{m=1}^{M} |x(m,n)| \tag{5}$$

where $x(m,n)$ is the set of wavelet coefficients, whose energy is being calculated, being m and n the indexes of the coefficients. Basing on the traditional definition of a calorie, the units of $\bar{\varepsilon}$ are wavelet calories (wCal) and can also be defined by Eq. 5, since a wCal is the energy needed to increase the absolute magnitude of a wavelet coefficient by one scale.

From wavelet coefficients $\{\omega_{s,o}\}$ and $\{\hat{\omega}_{s,o}\}$ the corresponding perceptual wavelet coefficients $\{\omega_{s,o;\rho,\tilde{d}}\} = \alpha(v,r) \cdot \omega_{s,o}$ and $\{\hat{\omega}_{s,o;\rho,\tilde{d}}\} = \alpha(v,r) \cdot \hat{\omega}_{s,o}$ are obtained by applying CIWaM with an observation distance $\tilde{d}$. Therefore Equation 6 expresses the relative wavelet energy ratio $\varepsilon R(\tilde{d})$, which compares how different are the energies of the reference and distorted CIWaM perceptual images, namely ε_ρ and ε_ρ respectively, when these images are watched from a given distance $\tilde{d}$.

$$\varepsilon\mathcal{R}\left(\tilde{d}\right) = 10 \cdot \left| \log_{10} \frac{\varepsilon_\rho\left(\tilde{d}\right)}{\hat{\varepsilon}_\rho\left(\tilde{d}\right)} \right| \tag{6}$$

Figure 3(a) shows that distance D is composed by the sum of two distances, nP and εmL. Thereby for the estimation of D, Eq. 7, it is necessary to know the observation distance d besides to figure out the nP and εmL distances. Furthermore Figure 3(b) depicts a chart of εR, which sketches both the behavior of the relative energy when $\tilde{d}$ is varied from 0 to ∞ centimeters and the meaning of the distances D, nP and εmL inside an εR chart.

$$D = nP + \varepsilon mL \tag{7}$$

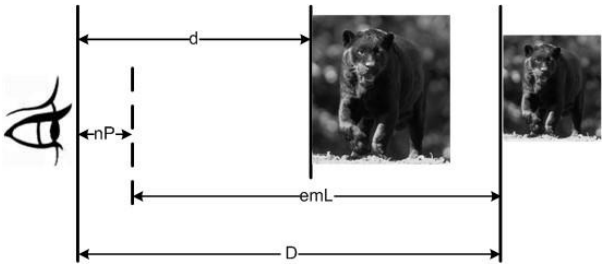

(a) Distances employed by the VPSNR algorithm.

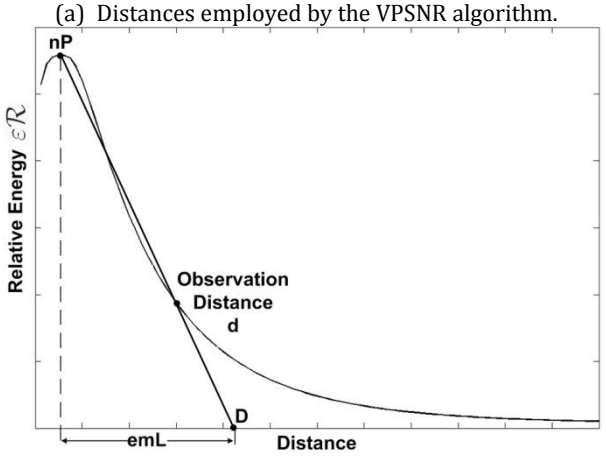

(b) εR Chart.

Fig.3. Definition of distances D, nP and εmL both graphically (a) and inside an εR Chart (b).

The peak inside an εR chart is nP, which is the distance where the observer is able to better assess the difference between the images $f(i,j)$ and $\hat{f}(i,j)$. From this point nP the observer starts to perceive fewer the differences, until in ∞ these differences disappear, in practice, this point varies from 15 to 25 centimeters. Our metrics is based on finding an approximation of the distance D where the wavelet energies are linearly the same, that is, $\varepsilon R(D) \approx 0$. This is achieved by projecting the points $(nP, \varepsilon R(nP))$ and $(d, \varepsilon R(d))$ to $(D,0)$.

Therefore εmL is the needed length to match the energies from the point where the observer has the best evaluation of the assessed images to D and is described as follows:

$$\varepsilon m\mathcal{L} = \frac{\varepsilon\mathcal{R}(n\mathcal{P})}{d\varepsilon\mathcal{R} + \varsigma} \tag{8}$$

where εR(nP) is the relative energy at nP and $d\varepsilon$R is the energy loss rate (wCal/cm or wCal/visual degrees) between (nP,εR(nP)) and (d,εR(d)), namely, the negative slope of the line joining these points, expressed as:

$$d\varepsilon\mathcal{R} = \frac{\varepsilon\mathcal{R}(n\mathcal{P}) - \varepsilon\mathcal{R}(d)}{d - n\mathcal{P}} \tag{9}$$

When a lossless compression is performed, consequently $f(i,j) = \hat{f}(i,j)$, hence $d\varepsilon$R = 0 and εmL → ∞. In order to numerically avoid it, parameter ς is introduced, which is small enough to not affect the estimation of εmL when $d\varepsilon$R ≠ 0, in our MatLab implementation ς = *realmin*.

Step 3: Perceptual Images

Obtain the perceptual wavelet coefficients $\{\omega_{s,o;\rho,D}\} = \alpha(v,r) \cdot \omega_{s,o}$ and $\{\hat{\omega}_{s,o;\rho,D}\} = \alpha(v,r) \cdot \hat{\omega}_{s,o}$ at distance D, using Equation 4.

Step 4: Inverse Wavelet Transformation

Perform the Inverse Wavelet Transform of $\{\omega_{s,o;\rho,D}\}$ and $\{\hat{\omega}_{s,o;\rho,D}\}$, obtaining the perceptual images $f_{\rho(i,j),D}$ and $\hat{f}_{\rho(i,j),D}$, respectively. The synthesis filter in Table 2 is an inverse Daubechies 9-tap/7-tap filter.

Table 2. 9/7 Synthesis Filter.

Synthesis Filter		
i	Low-Pass Filter $h_L(i)$	High-Pass Filter $h_H(i)$
0	1.115087052456994	0.6029490182363579
±1	0.5912717631142470	-0.2668641184428723
±2	-0.05754352622849957	-0.07822326652898785
±3	-0.09127176311424948	0.01686411844287495
±4		0.02674875741080976

Step 5: PSNR between perceptual images

Calculate the PSNR between perceptual images $f_{\rho(i,j),D}$ and $\hat{f}_{\rho(i,j),D}$ using Eq. 2 in order to obtain the CIWaM weighted PSNR i.e. the VPSNR.

2.3 Discussion

Figures 4(c) *Sailboat on Lake*$_2$ and 5(b) *Splash*$_1$ $D_2 = D_1 = 129cm$, but subjective quality of *Splash*$_1$ is clearly better than the one of *Sailboat on Lake*$_2$. Thus, even when CIWaM versions of *Splash*$_1$ and *Sailboat on Lake*$_2$ are calculate at 129*cm*, the

resultant perceptual images have different objective quality. Hence VPSNR predicts that the error in Figure 5(b) is twice less ($\sim 3dB$) than in Figure 4(c).

That is why overall VPSNR algorithm is the estimation of the objective quality taking into account the set of the interactions of parameters nP, d and D. Figures 5 and 6 show examples when perceptual quality is equal and their respective points (nP,εR(nP)) do not correspond. In Figure 5, there is a difference of $6cm$ between D_1 and D_2, while in Figure 6, there is no difference between distances D_1 and D_2.

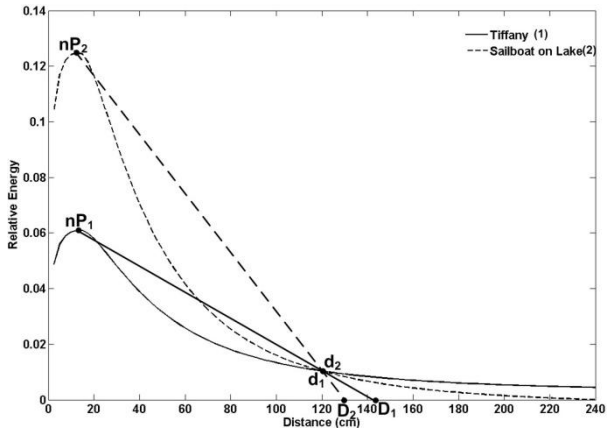

(a) Relative Energy Chart

(b) D_1=141.45cm
VPSNR=34.82dB

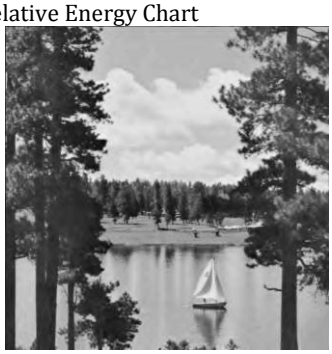

(c) D_2=129.67cm
VPSNR=36.77dB

Fig.4. Relative Energy Chart of Images *Tiffany* and *Sailboat on Lake* (a), which are distorted by means of JPEG2000 PSNR=31dB and Observation Distance d=120cm. Perceptual quality VPSNR is equal to 34.82dB for (b) and 36.77dB for (c).

3 Experimental results

In this section, VPSNR performance is assessed by comparing the statistical significance with the psychophysical results obtained by human observers when

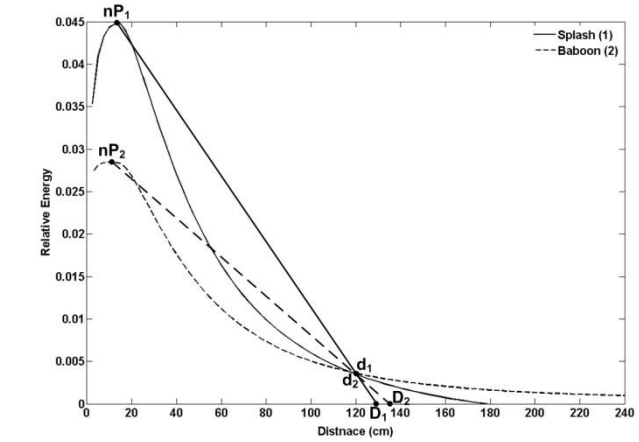

(a) Relative Energy Chart

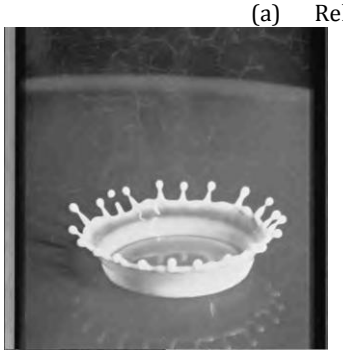

(b) D_1=129.10cm
PSNR=35.88dB

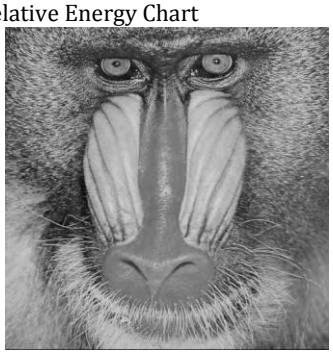

(c) D_2=135.89cm
PSNR=31.74dB

Fig.5. Relative Energy Chart of Images *Splash* and *Baboon*, which are distorted by means of JPEG2000 VPSNR=39.69dB and Observation Distance d=120cm. Objective quality PSNR is equal to 35.88dB for (b) and 31.74dB for (c).

judging the visual quality of an specific image. These results are expressed in Mean Opinion Scores. In this way, perceived image quality predicted by VPSNR is tested for JPEG2000 distortion across the Tampere Image Database (TID2008) of the Tampere University of Technology, presented by Ponomarenko et.al. in [9,10].

TID2008 Database contains 25 original images (Figure 7), which are distorted by 17 different types of distortions, each distortion has 4 degrees of intensity, that is, 68 versions of each source image. TID2008 also supplies subjective ratings by comparing original and distorted images by 654 observers from Italy, Finland and Ukraine. Thus, for JPEG and JPEG2000 compression distortions, there are 200 (25 images × 2 distortions × 4 distortion degrees) images in the database. MOS is presented as the global rating.

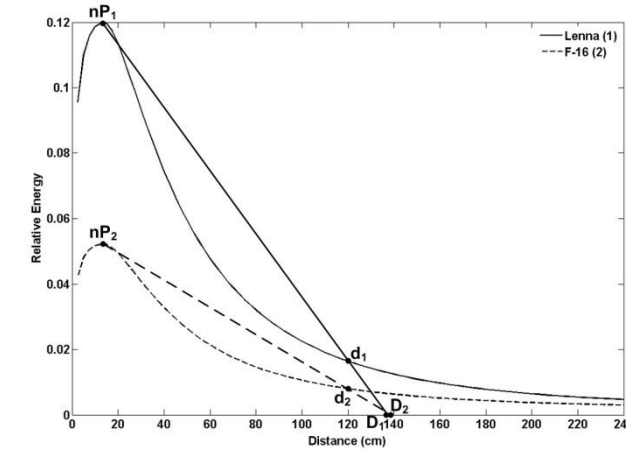

(a) Relative Energy Chart

(b) D_1=137.12cm
PSNR=31.00dB

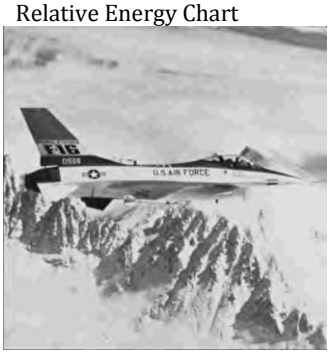

(c) D_2=139.49cm
PSNR=30.87dB

Fig.6. Relative Energy Chart of Images *Lenna* and *F-16*, which are distorted by means of JPEG2000 VPSNR=34.75dB and Observation Distance d=120cm. Objective quality PSNR is equal to 31.00dB for (b) and 30.87dB for (c).

3.1 Performance measures

Strength of Relationship (SR) is measured by a correlation coefficient. SR means how strong is the tendency of two variables to move in the same (opposite) direction. Pearson Correlation Coefficient (PCC) is the most common measure for predicting SR, when parametric data are used. But in the case of the correlation of non-parametric data the most common indicator is Spearman Rank-Order Correlation Coefficient (SROCC). Results of image quality metrics have no lineal relationship, which is why, it is not convenient to employ PCC, since even PSNR and MSE are the same metrics, PCC calculates different values.

Hence SROCC is a better choice for measuring SR between the opinion of observers and the results of a given metrics. However SROCC is appropriate for

Fig.7. Tested 512 × 384 pixel 24-bit color images, belonging to the Tampere Image Database.

testing a null hypothesis, but when this null hypothesis is rejected is difficult to interpret[11]. In the other hand, Kendall Rank-Order Correlation Coefficient (KROCC) corrects this problem by reflecting SR between compared variables. Furthermore KROCC estimates how similar are two rank-sets against a same object set. Thus, KROCC is interpreted as the probability to rank in the same order taking into account the number of inversions of pairs of objects for transforming one rank into the other[12]. Which is why, VPSNR and the rest of metrics are evaluated using KROCC. One of Limitation of KROCC is located in complexity of the algorithm, which takes more computing time than PCC and SROCC, but KROCC can show us an accurate Strength of Relationship between a metric and the opinion of an human observer.

MSE[13], PSNR[13], SSIM[14], MSSIM[15], VIF[16], VIFP[14], IFC[17] and WSNR[18] are compared against the performance of VPSNR for JPEG2000 compression distortion. I chose for evaluating these assessments the implementation provided in [19], since it is based on the parameters proposed by the author of each indicator.

VPSNR is implemented assuming the following features:

- Observation Distance, d=8H, where H is the height of a 512 × 512 image.
- 19" LCD monitor with horizontal resolution of 1280 pixels and 1024 pixels of vertical resolution.
- Gamma correction, $\gamma = 2.2$
- Wavelet Transform, set of wavelet planes ω with $n = 3$, Eq. 3.

3.2 Overall performance

Table 3 shows the performance of VPSNR and the other eight image quality assessments across the set of images from TID2008 image database employing KROCC for testing the distortion produced by a JPEG2000 compression.

Table 3. KROCC of VPSNR and other quality assessment algorithms on multiple image databases using JPEG2000 distortion. Bold and italicized entries represent the best and the second-best performers in the database, respectively. The last column shows the KROCC average of all image databases.

Metrics	TID2008 Image Database
Images	100
MSE	0.6382
PSNR	0.6382
SSIM	0.8573
MSSIM	*0.8656*
VIF	0.8515
VIFP	0.8215
IFC	0.7905
WSNR	0.8152
$\mathcal{V}$PSNR	**0.8718**

Thus, for JPEG2000 compression distortion, VPSNR is also the best metrics for each database. VPSNR gets its better results when correlation is 0.8718 for a corpus of 100 images of the TID2008 database. For this distortion, MSSIM is the second best indicator. Furthermore VPSNR improves 0.2336 the perceptual functioning of PSNR when this metrics compares perceptual images in a dynamic way.

4 Conclusion

In this work, I presented a new metrics of full-reference image quality based on perceptual weighting of PSNR by means of a perceptual model. The VPSNR metrics is based on the measurement the objective quality of perceptual images predicted by CIWaM at *D*.

VPSNR was tested in TID2008 image database, over viewing distances proposed in this image database. Results show that VPSNR significantly increases the correlation of PSNR with perceived image quality, maintaining its advantageous features, in addition to be the best-ranked image quality gauge in overall performance, in comparison to a diversity of existing metrics. Accuracy of Second best-performing algorithm, MSSIM, is 1.5% lower than VPSNR forJPEG2000 distortion. While when CIWaM weights PSNR correlation of predicting subjective ratings either of PSNR or MSE improves the results by 23.36% for the same kind of distortions, on the average.

VPSNR is mainly developed for optimizing the perceptual error under the constraint of a limited bit-budget, but it contains another properties that can be used for quantizing, since the CIWaM algorithm calculates one value of an extended contrast sensitivity function by pixel. In this way, it is possible to quantize a particular pixel while an algorithm of bit allocation is working, incorporating into embedded compression schemes such as EZW[20], SPIHT[21], JPEG2000[22] or H*i*-SET[23].

Acknowledgment

This work is supported by National Polytechnic Institute of Mexico by means of Project No. 20131312 granted by the Academic Secretary, National Council of Science and Technology of Mexico by means of Project No. 204151/2013, Coimbra Group Scholarship Programme granted by University of Poitiers and Region of Poitou-Charentes, France.

References

1. Z. Wang and A. Bovik, Mean squared error: Love it or leave it? a new look at signal fidelity measures, Signal Processing Magazine, IEEE, vol. 26, no. 1, pp. 98 –117, jan. (2009).
2. Z. Wang and A. C. Bovik, Modern Image Quality Assessment, 1st ed. Morgan & Claypool Publishers: Synthesis Lectures on Image, Video, & Multimedia Processing, February (2006).
3. F. Auli-Llinas and J. Serra-Sagrista, Low complexity JPEG2000 rate control through reverse subband scanning order and coding passes concatenation, IEEE Signal Processing Letters, vol. 14, no. 4, pp. 251 –254, april (2007).
4. D. S. Taubman and M. W. Marcellin, JPEG2000: Image Compression Fundamentals, Standards and Practice, ser. ISBN: 0-7923-7519-X. Kluwer Academic Publishers, 2002.
5. J. Bartrina-Rapesta, F. Auli-Llinas, J. Serra-Sagrista, and J. Monteagudo-Pereira, JPEG2000 Arbitrary ROI coding through rate-distortion optimization techniques, in Data Compression Conference, pp. 292 –301. (2008).
6. X. Otazu, C. Párraga, and M. Vanrell, Toward a unified chromatic induction model, Journal of Vision, vol. 10(12), no. 6, (2010).
7. G. van de Wouwer, P. Scheunders, and D. van Dyck, Statistical texture characterization from discrete wavelet representations, IEEE Transactions on Image Processing, vol. 8, no. 4, pp. 592 –598, Apr. (1999).

8. B. A. Wilson and M. A. Bayoumi, A computational kernel for fast and efficient compressed-domain calculations of wavelet subband energies, IEEE Transactions on Circuits and Systems II: Analog and Digital Signal Processing, vol. 50, no. 7, pp. 389 – 392, July (2003).
9. N. Ponomarenko, V. Lukin, A. Zelensky, K. Egiazarian, M. Carli, and F. Battisti, TID2008 - a database for evaluation of full-reference visual quality assessment metrics, Advances of Modern Radioelectronics, vol. 10, pp. 30–45, (2009).
10. N. Ponomarenko, F. Battisti, K. Egiazarian, J. Astola, and V. Lukin, Metrics performance comparison for color image database, Fourth international workshop on video processing and quality metrics for consumer electronics, p. 6 p., (2009).
11. M. Hollander and D. Wolfe, Non-parametric Statistical Methods, 2nd ed. Wiley, (1999).
12. H. Abdi, Kendall rank correlation., N. Salkind, Ed. Encyclopedia of Measurement and Statistics. Thousand Oaks (CA), (2007).
13. Q. Huynh-Thu and M. Ghanbari, Scope of validity of PSNR in image/video quality assessment, Electronics Letters, vol. 44, no. 13, pp. 800–801, (2008).
14. H. Sheikh and A. Bovik, Image information and visual quality, IEEE Transactions on Image Processing, vol. 15, no. 2, pp. 430 –444, feb. (2006).
15. Z. Wang, E. Simoncelli, and A. Bovik, "Multiscale structural similarity for image quality assessment, in Conference Record of the Thirty-Seventh Asilomar Conference on Signals, Systems and Computers., vol. 2, pp. 1398 – 1402, (2003).
16. Z. Wang, A. Bovik, H. Sheikh, and E. Simoncelli, Image quality assessment: from error visibility to structural similarity, IEEE Transactions on Image Processing, vol. 13, no. 4, pp. 600 –612, (2004).
17. R. Sheikh, A. Bovik, and G. de Veciana, An information fidelity criterion for image quality assessment using natural scene statistics, IEEE Transactions on Image Processing, vol. 14, pp. 2117–2128, (2005).
18. T. Mitsa and K. Varkur, Evaluation of contrast sensitivity functions for formulation of quality measures incorporated in halftoning algorithms, IEEE International Conference on Acustics, Speech and Signal Processing, vol. 5, pp. 301–304, (1993).
19. C. U. V. C. Laboratory: MeTriX MuX visual quality assessment package, available at http : //foulard.ece.cornell.edu/gaubatz/metrix mux/. Cornell University Visual Communications Laboratory. (2010).
20. J. Shapiro, Embedded image coding using Zerotrees of wavelet coefficients, IEEE Transactions on Acoustics, Speech, and Signal Processing, vol. 41, no. 12, pp. 3445 – 3462, (1993).
21. A. Said and W. Pearlman, A new, fast, and efficient image codec based on Set Partitioning In Hierarchical Trees, IEEE Transactions on Circuits and Systems for Video Technology, vol. 6, no. 3, pp. 243 – 250, (1996).
22. A. Skodras, C. Christopoulos, and T. Ebrahimi, The JPEG 2000 still image compression standard, IEEE Signal Processing Magazine, vol. 18, no. 5, pp. 36–58, (2001).
23. J. Moreno and X. Otazu, "Image coder based on Hilbert Scaning of Embedded quadTrees," IEEE Data Compression Conference, p. 470, (2011).